EurJIC
European Journal of Inorganic Chemistry

Research Article
doi.org/10.1002/ejic.202300099

Chemistry Europe
European Chemical Societies Publishing

www.eurjic.org

Prizewinner Collection

Bimetallic Carbonyl Complexes Based on Iridium and Rhodium: Useful Tools for Hydrodefluorination Reactions

Konrad Kretschmar,[a] Vladimir Pelmenschikov,[b] Martin Kaupp,*[b] Thomas Braun,*[a] Philipp Wittwer,[a] Simon Rachor,[a] and Jesvita Cardozo[a]

A set of bimetallic complexes based on iridium and rhodium with bis(diphenylphosphino)methane, bis(di-*iso*-propylphosphino)methane, diphenyl-2-pyridylphosphine and 2-(di-*iso*-propylphosphino)imidazole bridging ligands was prepared. The complexes were characterized by NMR and IR spectroscopy and studied quantum-chemically using DFT methods. The bimetallic systems succeeded in catalytic hydrodefluorination reactions of lower fluorinated aryl fluorides using molecular hydrogen and sodium *tert*-butoxide as a base. Effects of (*i*) ligand variation, (*ii*) mono- vs bimetallic nuclearity, and (*iii*) Ir vs Rh metal identity were studied and rationalized en route to achieve an effective hydrodefluorination.

Introduction

Bimetallic transition metal complexes gain increasing attention due to their potential for unique reactivities and selectivities that may be absent for respective mononuclear metal catalysts.[1] For instance, heterobinuclear complexes bearing two different metal centers can afford catalytic conversion in a cooperative way. A wide variety of late-late transition metal complexes were synthesized by using bridging ligands such as bis(diphosphino)methane[2] or 2-(diphenylphosphino)pyridine (PPh_2py).[1m,3] Cowie et al. reported several compounds characterized by various metal combinations including Ir/Ir,[2c,o] Rh/Rh,[4] Ir/Rh,[2c,e,i,k,o,p] Ir/Ru,[2m,n] and Ir/Os.[2f,g,m] The Ir/Ir carbonyl complexes $[Ir_2(CH_3)(CO)_2(dppm)_2][CF_3SO_3]$ (dppm = bis(diphenylphosphino)methane) and $[Ir_2(CO)_3(\mu\text{-}H)(depm)_2][BAr^F{}_4]$ (depm = bis(diethylphosphino)methane enabled the C–F bond activation reactions of various polyfluorinated ethylene derivatives.[5] Heterobimetallic complexes (Ir/Pd or Ru/Pd) bearing 1,2,4-triazolyl-3,5-dilyidene ligands were superior when compared to the monometallic or homobimetallic counterparts in catalytic tandem reactions,[1e] such as Suzuki-Miyaura couplings and transfer hydrogenations,[1c] as well as hydrodefluorination and transfer hydrogenation reactions.[1a] In the last decade, three different bimetallic systems have been used to achieve hydrodefluorination reactions of lower fluorinated aryl fluorides using sodium *tert*-butoxide as a base and a hydrogen source (Scheme 1).[1a,b,n] A Ru/Pd based catalyst was capable of hydrodefluorination of fluorobenzenes to yield benzene when using *i*PrOH as hydrogen source at 80 °C. It was proposed that the Ru center facilitates the dehydrogenation of *i*PrOH, and the Pd site mediates the C–F bond activation.[1a] For an In/Rh system dihydrogen was used as hydrogen source. The In-containing moiety was introduced as a σ-acceptor Z-type ligand to stabilize a reactive Rh(–I) species, which is responsible for cleaving the C–F bond. Corresponding Al/Rh and Ga/Rh bimetallic complexes were less active in thermal hydrodefluorination reactions, and it was proposed that the electronic properties of the system can be tuned by the right choice of the main group metal.[1b] The Ga/Rh bimetallic system was also applied to achieve the C–F bond activation under photolytic conditions.[1n] Commonly, monometallic systems are used to achieve hydrodefluorination of aryl fluorides at aromatics, and the C–F bond

[a] K. Kretschmar, Prof. Dr. T. Braun, Dr. P. Wittwer, S. Rachor, J. Cardozo
Humboldt-Universität zu Berlin,
Institut für Chemie
Brook-Taylor-Straße 2, 12489 Berlin (Germany)
E-mail: thomas.braun@cms.hu-berlin.de
[b] Dr. V. Pelmenschikov, Prof. Dr. M. Kaupp
Institut für Chemie,
Technische Universität Berlin,
Theoretische Chemie/Quantenchemie, Sekr.C7
Straße des 17. Juni 135, 10623 Berlin (Germany)
E-mail: martin.kaupp@tu-berlin.de

Supporting information for this article is available on the WWW under https://doi.org/10.1002/ejic.202300099

Part of the Wöhler Vereinigung für Anorganische Chemie Prize Winners Special Collection.

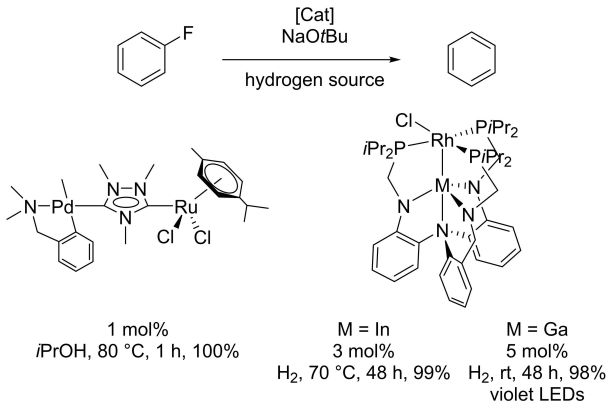

Scheme 1. Heterobimetallic Ru/Pd, In/Rh and Ga/Rh complexes previously reported for the hydrodefluorination of fluorobenzene.[1a,b]

Research Article
doi.org/10.1002/ejic.202300099

activation is promoted by the formation of stable bonds, such as H–F, Al–F, B–F or Si–F bonds among others.[6]

Herein, we report on the synthesis, spectroscopic characterization, and density functional theory (DFT) calculations of bimetallic complexes bearing Ir and/or Rh centers bridged by bidentate phosphine ligands. Catalytic hydrodefluorination of aryl C–F bonds was achieved, and activities were observed under one atmosphere of dihydrogen using sodium *tert*-butoxide as stoichiometric base.

Results and Discussion

Treatment of $[Ir(\mu\text{-Cl})(COD)]_2$ with four equivalents of either bis(diphenylphosphino)methane (dppm), bis(di-*iso*-propylphosphino)methane (dippm), diphenyl-2-pyridylphosphine (PPh_2py) or 2-(di-*iso*-propylphosphino)imidazole ($PiPr_2Im$d) and subsequently with CO led to the formation of the mononuclear Ir(I) complexes $[Ir(CO)(dppm)_2]Cl$ (**1a**$_{Ir}$), $[Ir(CO)(dippm)_2]Cl$ (**1b**$_{Ir}$), *trans*-$[IrCl(CO)(PPh_2py)_2]$ (**1c**$_{Ir}$) and *trans*-$[IrCl(CO)(PiPr_2Im$d$)_2]$ (**1d**$_{Ir}$) (Scheme 2). The complexes **1a**$_{Ir}$ and **1c**$_{Ir}$ have been reported before, but were synthesized via a different reaction route.[3b,7] Additionally, Vaska-type complexes $[Ir(CO)L_2X]$ (L = phosphine, X = halide) similar to **1d**$_{Ir}$ have been recently reported.[8] All complexes were characterized by ^{1}H NMR, $^{31}P\{^1H\}$ NMR and IR spectroscopy (see Supporting Information). The $^{31}P\{^1H\}$ NMR spectra of the complexes **1a**–**d**$_{Ir}$ reveal a singlet for the phosphorus atoms of the phosphine ligands. The signals of the complexes **1a**$_{Ir}$ appear at $\delta = -56.9$ ppm and **1b**$_{Ir}$ at $\delta = -46.6$ ppm, whereas the complexes **1c**$_{Ir}$ show resonances at $\delta = 37.9$ ppm and **1d**$_{Ir}$ at $\delta = 28.9$ ppm. The ^{1}H NMR spectrum of **1d**$_{Ir}$ reveals a broad signal for the NH group at $\delta = 11.47$ ppm. The resonance appears at higher field when compared to the data for the free phosphine ($\delta = 11.74$ ppm).[9] The IR spectrum of **1d**$_{Ir}$ shows a very broad absorption band at $\tilde{\nu} = 3343$ cm^{-1} for the N–H moiety. The N–H absorption frequency of the phosphine $PiPr_2Im$d (3090 cm^{-1}) exhibits broad absorption bands at lower frequencies, which can be tentatively explained by (stronger) hydrogen bonding interactions in the free phosphine. For all four complexes **1a**–**d**$_{Ir}$, very intense absorption bands for the CO stretching modes were detected in the ATR IR spectra (1926 cm^{-1} for **1a**$_{Ir}$, 1922 cm^{-1} for **1b**$_{Ir}$, 1971 cm^{-1} for **1c**$_{Ir}$[3b] and 1944 cm^{-1} for **1d**$_{Ir}$), which is consistent with data of other iridium-based Vaska type complexes.[10]

Attempts were also made to synthesize the monometallic rhodium complexes corresponding to **1a**–**d**$_{Ir}$. Unfortunately, only the known complex *trans*-$[RhCl(CO)(PPh_2py)_2]$ (**1c**$_{Rh}$) could be obtained analytically pure by a synthetic route similar to the described synthesis of complex **1c**$_{Ir}$.[11] The formation of complex $[Rh(CO)(dppm)_2]Cl$ (**1a**$_{Rh}$) was observed in solution and **1a**$_{Rh}$ was used for the synthesis of the bimetallic complex $[IrRh(Cl)_2(\mu\text{-CO})(dppm)_2]$ (**2a**$_{IrRh}$) described below (Scheme 3). However, when trying to isolate the complex **1a**$_{Rh}$ by recrystallization, the compound started to decompose. The IR spectra of the **1a**$_{Rh}$ sample shows a vibrational band at $\tilde{\nu} = 1936$ cm^{-1} comparable to the one for complex $[Rh(CO)(dppm)_2]BF_4$ (1945 cm^{-1})[12] and a smaller band at $\tilde{\nu} = 1968$ cm^{-1}. The $^{31}P\{^1H\}$ NMR spectrum of **1a**$_{Rh}$ shows a very broad doublet at $\delta = -21.4$ ppm. An attempt to prepare the rhodium complex $[Rh(CO)(dippm)_2]Cl$ (**1b**$_{Rh}$) by a similar procedure used for the iridium complex **1b**$_{Ir}$ led to the formation of $[Rh(dippm)_2]Cl$[13] instead due to the loss of CO. At last, many attempts using different solvents to synthesize the rhodium analogue of **1d**$_{Ir}$, *trans*-$[RhCl(CO)(PiPr_2Im$d$)_2]$ (**1d**$_{Rh}$),

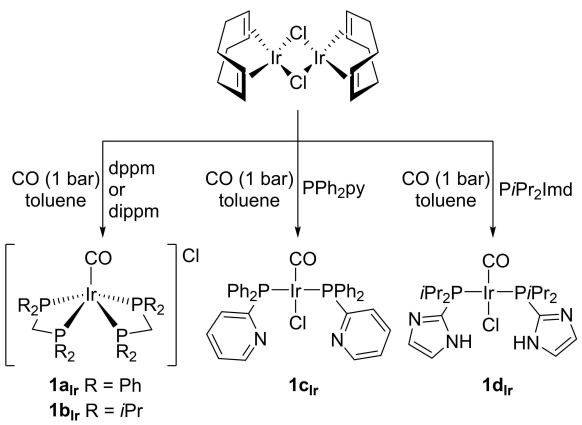

Scheme 2. Synthesis of the monometallic Ir(I) carbonyl phosphine complexes.

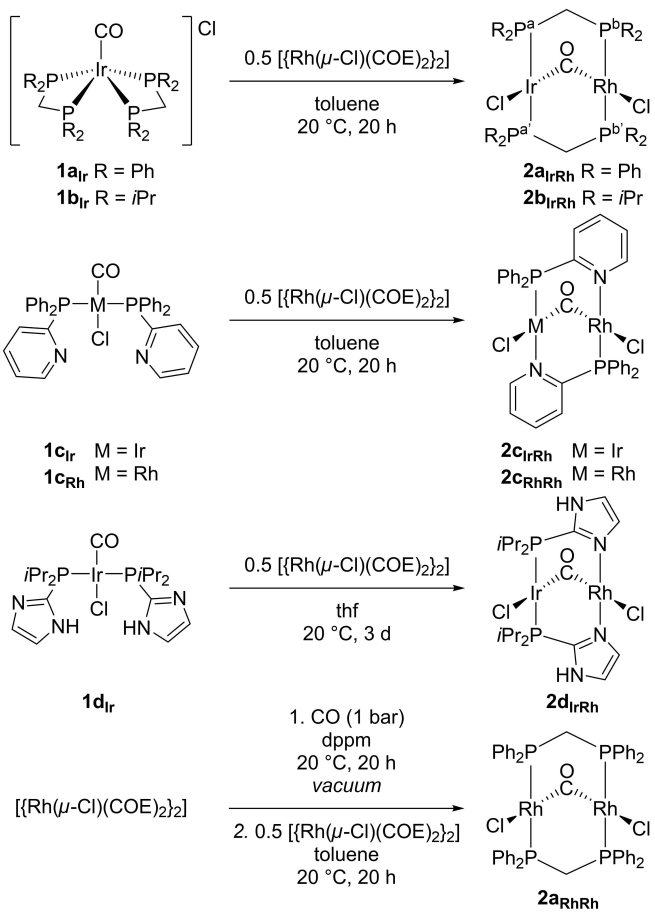

Scheme 3. Synthesis of **2a**$_{RhRh}$ and heterobimetallic Ir(I)/Rh(I) complexes.[11]

Research Article
doi.org/10.1002/ejic.202300099

failed, which is most likely due cyclometallation of the imidazole moiety of the ligand.[8]

The structures of the complexes **1a**–**c**$_{Ir}$ were determined by X-ray crystallography, as depicted in Figures 1–3. Selected bond lengths, angles and other interatomic distances are given in the captions of the corresponding figures. Compound **1a**$_{Ir}$ crystallized with a water molecule in the asymmetric unit. The structures of the cations in **1a**$_{Ir}$ and **1b**$_{Ir}$ exhibit an arrangement intermediate between trigonal bipyramidal and square pyramidal as reported for [Ir(CO)(dppe)$_2$]Cl (dppe = bis(diphenylphosphino)ethane).[14] The geometry parameter τ_5[15] reveals that the structure of **1b**$_{Ir}$ ($\tau_5 = 0.37$) is closer to a square-pyramidal coordination than the structure of **1a**$_{Ir}$ ($\tau_5 = 0.53$). The molecular structure of **1c**$_{Ir}$ exhibits a metal-ligand core with structural parameters very similar to the Vaska complex [Ir(CO)(Cl)(PPh$_3$)$_2$].[16] DFT modeling (see Supporting Information) reproduced the structural parameters of the X-ray data of **1a**–**c**$_{Ir}$ very well, and offered a prediction for the structure of **1d**$_{Ir}$ (Figure S39). As detailed in Table S2, the Ir bound CO stretching mode frequencies observed by IR spectroscopy (1922–1971 cm^{-1}) were also reproduced by the calculated values (1910–1963 cm^{-1}) within a ~50 cm^{-1} range. The DFT models of the monometallic rhodium complexes **1a**$_{Rh}$ and **1c**$_{Rh}$ were based on their iridium analogues and mirrored the experimentally observed CO IR band energies with a deviation of 6 cm^{-1} at most.

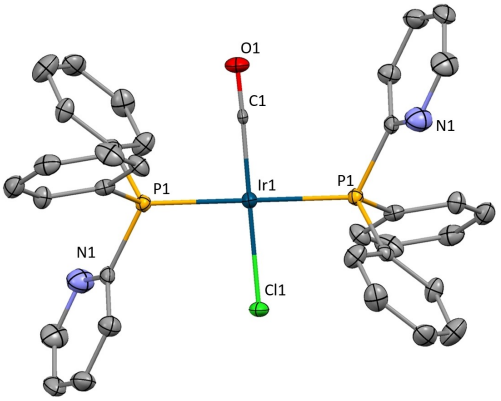

Figure 3. Molecular structure of [Ir(CO)(Cl)(PPh$_2$py)$_2$] (**1c**$_{Ir}$). Thermal ellipsoids are drawn at 50% probability level. Carbon bound hydrogen atoms and the non-interacting CH_2Cl_2 solvent molecule were omitted for clarity. Selected bond lengths [Å] and bond angles [°]: Ir1–C1 1.785(8); Ir1–P1 2.3116(6); Ir1–Cl1 2.373(3); C1–Ir1–P1 92.5(4); P1–Ir1–P1 180.0; C1–Ir1–Cl1 179.3(4).

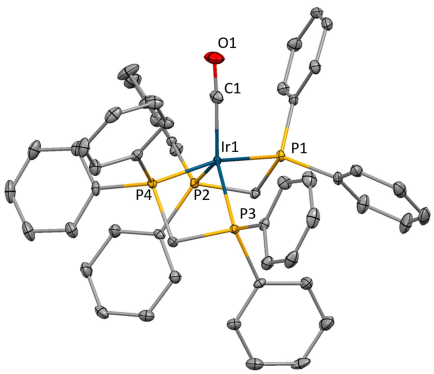

Figure 1. Structure of the cation in [Ir(CO)(dppm)$_2$]Cl·H$_2$O (**1a**$_{Ir}$). Thermal ellipsoids are drawn at 50% probability level. Carbon bound hydrogen atoms were omitted for clarity. Selected bond lengths [Å] and bond angles [°]: Ir1–C1 1.887(2); Ir1–P1 2.3222(9); Ir1–P2 2.3515(11); Ir1–P3 2.3770(9); Ir1–P4 2.3079(10); C1–O1 1.154(3); C1–Ir1–P4 98.59(6); C1–Ir1–P1 95.54(6); P4–Ir1–P1 165.580(18); C1–Ir1–P2 118.85(7); P4–Ir1–P2 100.25(4); P1–Ir1–P2 70.11(4); C1–Ir1–P3 133.92(6); P4–Ir1–P3 70.44(3); P1–Ir1–P3 101.54(3); P2–Ir1–P3 107.20(4); O1–C1–Ir1 175.98(19).

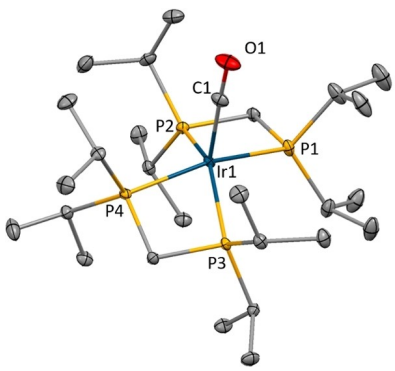

Figure 2. Structure of the cation in [Ir(CO)(dippm$_2$]Cl (**1b**$_{Ir}$). Thermal ellipsoids are drawn at 50% probability level. Carbon bound hydrogen atoms and the non-interacting CH_2Cl_2 solvent molecule were omitted for clarity. Selected bond lengths [Å] and bond angles [°]: Ir1–C1 1.9040(16); Ir1–P2 2.3368(4); Ir1–P4 2.3443(4); Ir1–P3 2.3457(4); Ir1–P1 2.3577(4); O1–C1 1.150(2); C1–Ir1–P2 96.59(5); C1–Ir1–P4 98.49(5); P2–Ir1–P4 164.849(14); C1–Ir1–P3 110.02(5); P2–Ir1–P3 105.275(15); P4–Ir1–P3 70.764(14); C1–Ir1–P1 107.61(5); P2–Ir1–P1 70.872(15); P4–Ir1–P1 102.947(15); P3–Ir1–P1 142.359(14); O1–C1–Ir1 178.13(15).

Treatment of the iridium complexes **1a**–**d**$_{Ir}$ with [{Rh(μ-Cl)(COE)$_2$}$_2$] led to formation of the corresponding bimetallic complexes [IrRh(Cl)$_2$(μ-CO)(dppm)$_2$] (**2a**$_{IrRh}$), [IrRh(Cl)$_2$(μ-CO)(dippm)$_2$] (**2b**$_{IrRh}$), [IrRh(Cl)$_2$(μ-CO)(PPh$_2$py)$_2$] (**2c**$_{IrRh}$) and [IrRh(Cl)$_2$(μ-CO)(P*i*Pr$_2$Imd)$_2$] (**2d**$_{IrRh}$) (Scheme 3). For the synthesis of compound **2c**$_{IrRh}$, the homobimetallic complex [Rh$_2$(Cl)$_2$(μ-CO)(PPh$_2$py)$_2$] (**2c**$_{RhRh}$) was also always formed additionally as a minor product (**2c**$_{IrRh}$:**2c**$_{RhRh}$, 92:8). Unfortunately, the solubilities of both bimetallic complexes are comparable, and they could not be separated, neither by recrystallization nor by solvent extraction. By cooling the reaction to −50 °C, **2c**$_{IrRh}$ was obtained with 8% impurity of **2c**$_{RhRh}$ (estimated by ^{1}H NMR spectroscopy, see Supporting Information). Furthermore, the isotopologue of **2d**$_{IrRh}$ [IrRh(Cl)$_2$(μ-^{13}CO)(P*i*Pr$_2$Imd)$_2$] (**2d'**$_{IrRh}$) was obtained when *trans*-[IrCl(^{13}CO)(P*i*Pr$_2$Imd)$_2$] (**1d'**$_{IrRh}$) was treated with [{Rh(μ-Cl)(COE)$_2$}$_2$]. By mixing a solution of **1a**$_{Rh}$ with [{Rh(μ-Cl)(COE)$_2$}$_2$], the known homobimetallic complex [Rh$_2$(Cl)$_2$(μ-CO)(dppm)$_2$] (**2a**$_{RhRh}$)[4] was obtained in good yields (Scheme 3). The literature-known complex [Rh$_2$(Cl)$_2$(μ-CO)(PPh$_2$py)$_2$] (**2c**$_{RhRh}$) was also synthesized (Scheme 3) and used as precatalyst for the hydrodefluorination reactions described below.[11]

All binuclear complexes were characterized by ^{1}H NMR, ^{31}P{^{1}H} NMR and IR spectroscopy. The ^{31}P{^{1}H} NMR spectra of **2a**$_{IrRh}$ and **2b**$_{IrRh}$ feature AA'BB'X spin systems for the phosphine moieties bound to iridium and rhodium (**2a**$_{IrRh}$, δ(PRh) = 23.7 ppm, δ(PIr) = 14.2 ppm and **2b**$_{IrRh}$, δ(PRh) = 44.0 ppm, δ(PIr) = 29.9 ppm). The ^{31}P{^{1}H} spectra were simulated and the

Research Article
doi.org/10.1002/ejic.202300099

chemical shifts of the signals are comparable to those of other Ir/Rh bimetallic complexes.[2a,d,o] (Figure 4). The $^2J_{P,P}$ coupling constants of the phosphorus atoms in a mutually *trans* position appear in a typical range (349–436 Hz).[17] The $^1J_{P,Rh}$ couplings (**2a**$_{IrRh}$, $^1J_{P,Rh}$ = 122 Hz and **2b**$_{IrRh}$, $^1J_{P,Rh}$ = 120 Hz) are also comparable to the ones found for square-planar Rh(I) carbonyl chlorido compounds.[2o,18] The $^{31}P\{^1H\}$ NMR spectrum of the complex **2c**$_{IrRh}$ reveals two doublets of doublets. The signal at δ = 52.5 ppm ($^1J_{P,Rh}$ = 148 Hz, $^4J_{P,P}$ = 17 Hz) can be assigned to the Rh(I)-bound phosphine atom. Notably, the phosphine rhodium coupling is larger than for the monometallic complex [Rh(CO)(Cl)(PPh$_2$py)$_2$] (**1c**$_{Rh}$) ($^1J_{P,Rh}$ = 128 Hz).[19] The second signal at δ = 12.6 ppm can be assigned to the Ir(I)-bound phosphine atom with a small $^3J_{P,Rh}$ coupling constant of 5 Hz. The $^4J_{P,P}$ coupling constant of 17 Hz is consistent with values reported for **2c**$_{RhRh}$ ($^1J_{P,Rh}$ = 144 Hz, $^4J_{P,P}$ = 16 Hz, $^3J_{P,Rh}$ = 7 Hz).[11] The ^1H NMR spectrum of complex **2d**$_{IrRh}$ features a broad signal for the proton of the NH group at δ = 11.85 ppm that is more downfield shifted than the signal for the NH group of the monometallic complex **1d**$_{Ir}$ (δ = 11.47 ppm). Furthermore, the IR spectrum of **2d**$_{IrRh}$ reveals a very broad absorption band at $\tilde{\nu}$ = 3128 cm^{-1} for the N–H moiety, which is shifted to lower frequency compared to the N–H absorption frequency of **1d**$_{Ir}$ at 3343 cm^{-1}. Both absorption bands indicate the presence of hydrogen bonding.[9] The $^{31}P\{^1H\}$ NMR spectrum of **2d**$_{IrRh}$ exhibits a doublet at δ = 23.0 ppm ($^3J_{P,Rh}$ = 3 Hz). An additional doublet with a $^2J_{P,C}$ of 6 Hz was detected in the $^{31}P\{^1H\}$ NMR spectrum of the ^{13}CO-isotopologue **2d'**$_{IrRh}$.[20] A doublet of triplets ($^1J_{C,Rh}$ = 41 Hz, $^2J_{C,P}$ = 6 Hz) in the $^{13}C\{^1H\}$ NMR spectrum at δ = 218.5 ppm can be attributed to the ^{13}CO ligand. The downfield shift is due to the bridging nature of the CO ligand.[21] The $^{31}P\{^1H\}$ NMR spectrum of **2a**$_{RhRh}$ reveals an AA'A''A'''X pattern at δ = 20.5 ppm for the four phosphines instead of the reported doublet.[4] The ATR IR spectra of the complexes **2a–c**$_{IrRh}$ show vibrational bands for the bridging CO ligands at 1735 cm^{-1} for **2a**$_{IrRh}$, 1729/1722 cm^{-1} for **2b**$_{IrRh}$, and 1772 cm^{-1} for **2c**$_{IrRh}$. For **2d**$_{IrRh}$, an absorption band shifted to lower frequency at 1699 cm^{-1} was found. However, in thf solution two bands were found at 1703 cm^{-1} and 1760 cm^{-1} (Figure S27). The former can be attributed to molecules that exhibit intermolecular hydrogen bonding (see below). For the homobimetallic Rh/Rh complexes, the CO bands at 1750 cm^{-1} for **2a**$_{RhRh}$ and 1790 cm^{-1} for **2c**$_{RhRh}$ are shifted to higher frequency with respect to the corresponding bands of their Ir/Rh analogues.[21]

Single crystals of complexes **2a**$_{IrRh}$ and **2c**$_{IrRh}$ were obtained and the structures were determined by X-ray diffraction, but the quality of the obtained data sets is poor. For both structures the metal centers are disordered (Rh:Ir, **2a**$_{IrRh}$ 47:53, **2c**$_{IrRh}$ 48:52) (Figures 5 and 6). The molecular structures exhibit approximately square-planar geometries about each metal center, with the two coordination planes inclined towards each other through the

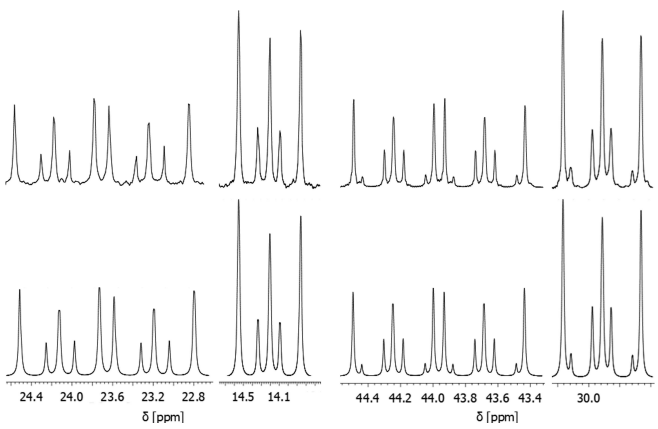

Figure 4. Simulated (bottom) and experimental (top) $^{31}P\{^1H\}$ NMR spectra of [IrRh(Cl)$_2$(μ-CO)(dppm)$_2$] (**2a**$_{IrRh}$) (left) and [IrRh(Cl)$_2$(μ-CO)(dippm)$_2$] (**2b**$_{IrRh}$) (right). The following coupling constants were obtained from the simulation (labels in Scheme 3): **2a**$_{IrRh}$, δ = 23.7 ($^2J_{Pa,Pa'}$ = 433.5, $^2J_{Pa,Pb}$ = 81.2, $^4J_{Pa',Pb}$ = 20.7, $^1J_{b,Rh}$ = 122.3 Hz) and 14.9 ($^2J_{Pb,Pb'}$ = 403.5, $^2J_{Pa,Pb}$ = 81.2, $^4J_{Pa',Pb}$ = 20.7, $^3J_{Pa,Rh}$ = -1.9 Hz) ppm; **2b**$_{IrRh}$ δ = 43.9 ($^2J_{Pa,Pa'}$ = 377.3, $^2J_{Pa,Pb}$ = 75.3, $^4J_{Pa',Pb}$ = 29.5, $^1J_{Pb,Rh}$ = 118.9 Hz) and 29.9 ($^2J_{Pb,Pb'}$ = 348.6, $^2J_{Pa,Pb}$ = 75.3, $^4J_{Pa',Pb}$ = 29.5, $^3J_{Pa,Rh}$ = -0.6 Hz) ppm.

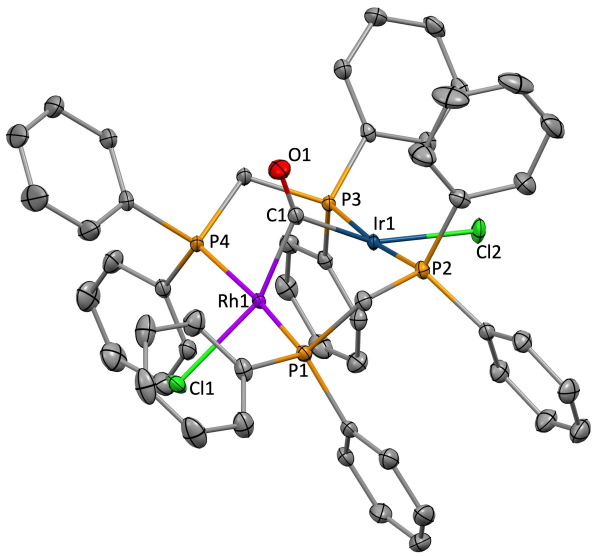

Figure 5. Molecular structure of [IrRh(Cl)$_2$(μ-CO)(dppm)$_2$] (**2a**$_{IrRh}$). Thermal ellipsoids are drawn at 50% probability level. Carbon bound hydrogen atoms and the non-interacting CH_2Cl_2 solvent molecule were omitted for clarity.

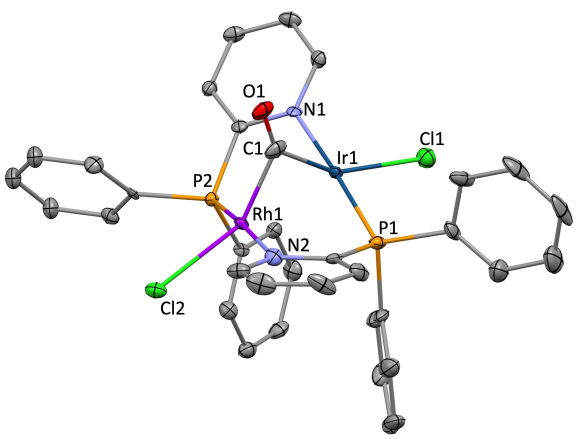

Figure 6. Molecular structure of [IrRh(Cl)$_2$(μ-CO)(PPh$_2$py)$_2$]·(**2c**$_{IrRh}$). Thermal ellipsoids are drawn at 50% probability level. Carbon bound hydrogen atoms and the four non-interacting C_6H_6 molecules were omitted for clarity.

Research Article
doi.org/10.1002/ejic.202300099

bridging carbonyl ligand. The eight-membered $RhIrP_4C_2$ ring or $RhIrP_2N_2C_2$ ring adopt a twisted boat-like conformation, such that the CH_2 groups of **2a$_{IrRh}$** and pyridyl moieties of **2c$_{IrRh}$** are oriented towards the bridging carbonyl group. Similar distorted A-frame boat conformations with bridging carbonyl or halogen ligands have been determined for other binuclear complexes.[2l,s,22]

Structural and vibrational properties of the bimetallic complexes relevant to the experiment were further addressed using their DFT models shown in Figure S40. An increase of ~0.1 Å in the DFT-optimized Ir/Rh–Rh distances (2.67–2.79 Å, **2c$_{RhRh}$** < **2c$_{IrRh}$** < **2d$_{IrRh}$** < **2a$_{RhRh}$** < **2a$_{IrRh}$** < **2b$_{IrRh}$**, Table S2) is correlated with a ~60 cm^{-1} shift to lower frequency of the metal-bridging CO stretching frequencies (1794–1732 cm^{-1}, **2c$_{RhRh}$** > **2c$_{IrRh}$** > **2d$_{IrRh}$** ≈ **2a$_{RhRh}$** > **2a$_{IrRh}$** > **2b$_{IrRh}$**, Table S2) across the six bimetallic complexes shown in Scheme 3, all having the [(Ir/Rh)Rh(Cl)$_2$(μ-CO)] fragment in common. Except for **2d$_{IrRh}$** (as explained below), this arrangement of the calculated CO frequencies mirrors the order of the experimental IR bands. The diminishing CO frequency values are accompanied by a fine 0.012 Å extension of the C–O bond length. At the same time, the Ir/Rh–CO distances remain uncorrelated and display only a small spread of 0.04 Å. DFT calculations also reproduce the observed ~20 cm^{-1} CO frequency shifts between **2a$_{IrRh}$** and **2c$_{IrRh}$** vs their homobimetallic analogues **2a$_{RhRh}$** and **2c$_{RhRh}$**, see Table S2, and associate it with a fine 0.005 Å extension of the C–O bond length upon exchange of Ir to Rh as the 2nd metal center.

Complex **2d$_{IrRh}$**, which evaded successful crystallization, constitutes a special case. The calculations initially predicted its metal-bridging CO frequency notoriously overestimated by ~50 cm^{-1} when compared to the band at 1699 cm^{-1} in the ATR IR specrum. In absence of an experimental structure, we speculate that a strong intermolecular hydrogen bonding to the CO oxygen is present in the solid sample of **2d$_{IrRh}$**. An addition of either water (CO···H_2O, **2d$_{IrRh}^{H2O}$**) or imidazole (CO···HN(Im), **2d$_{IrRh}^{Im}$**) molecule to the model (Figure S40) resulted in a shift of the CO frequency to a lower vibrational energy (Table S2). Among the two candidates, the model **2d$_{IrRh}^{Im}$** provided a better match of 1695 cm^{-1} to the IR band in the solid at 1699 cm^{-1} and the band at 1703 cm^{-1} in solution. An interaction of the metal-bound CO with a polar (Im)NH moiety from a neighboring molecule of the same species is therefore our most viable explanation for the low CO vibrational energy in **2d$_{IrRh}$**, among the bimetallic species studied. This is in line with the ^{1}H NMR and IR spectroscopic data for the NH moiety in **2d$_{IrRh}$** (see above).

Activation of molecular hydrogen by the bimetallic complexes **2a–d$_{IrRh}$**, **2a$_{RhRh}$** and **2c$_{RhRh}$** was studied, which might be of interest for hydrodefluorination reactions.[23] Treatment of **2b$_{IrRh}$** with H_2 led to formation of the dihydrido complex [IrRh(Cl)$_2$(H)(μ-H)(μ-CO)(dippm)$_2$] (**3**) (Scheme 4). In contrast, exposure of the remaining heterobimetallic complexes **2a$_{IrRh}$**, **2c$_{IrRh}$** and **2d$_{IrRh}$** to H_2 led only to their decomposition. When both homobimetallic complexes **2a$_{RhRh}$** and **2c$_{RhRh}$** were treated with H_2, no reaction occurred even after 14 days of exposure. The $^{31}P\{^1H\}$ NMR spectrum of compound **3** shows an AA'BB'X pattern for the phosphine moieties bound to iridium and rhodium (δ(PRh) = 48.7 ppm, δ(PIr) = 19.7 ppm). The $^1J_{P,Rh}$ coupling constant of complex **3** is only 10 Hz lower than for the starting compound

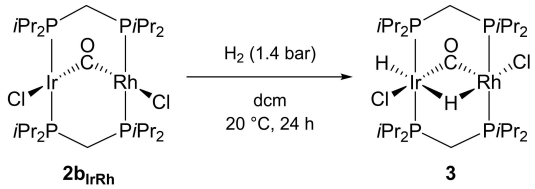

Scheme 4. Activation of molecular hydrogen by **2b$_{IrRh}$**.

2b$_{IrRh}$, indicating that the rhodium center remains in the oxidation state +I.[18,24] The ^{1}H NMR spectrum of **3** features a triplet of doublet at $\delta = -8.21$ ppm for the terminal hydrido ligand bound to iridium and a multiplet at $\delta = -16.37$ ppm for the bridging hydrido ligand. Decoupling of phosphorus nuclei led to doublets showing a coupling of both hydrido ligands to rhodium ($^3J_{H,Rh} = 4$ Hz for IrH and $^1J_{H,Rh} = 29$ Hz for μ-H). Notably, no coupling between the two hydrido ligands was detected, which is a known phenomenon for diphosphine-bridged A-frame hydrides of iridium.[2o,25] The IR spectra of **3** shows a vibrational band for the bridging CO ligand at 1761 cm^{-1}; the corresponding DFT-calculated $\tilde{\nu}$(CO) frequency appears at 1762 cm^{-1}.

Structural determination of **3** by X-ray crystallography (Figure 7) revealed an iridium-rhodium distance of 2.83 Å and showed that the carbonyl ligand is bonded more closely to the iridium than to the rhodium center (Ir–C = 1.93 Å; Rh–C = 2.04 Å). The positions of the hydrido ligands were fixed at a given position and refined with restraints. The DFT modelling of **3** (Figure S41) are in accordance with the data (Ir–Rh = 2.84, Ir–C = 1.95, Rh–C = 2.08 Å), and also suggest the *trans* positions of the hydrido ligands (with the metal-hydrido bonding parameters refined to Ir/Rh-μH = 1.84/1.71 Å for the bridging, and Ir–H = 1.62 Å for the terminal hydrides).

The bimetallic complexes prepared were then investigated towards their catalytic activity in hydrodefluorination reactions of

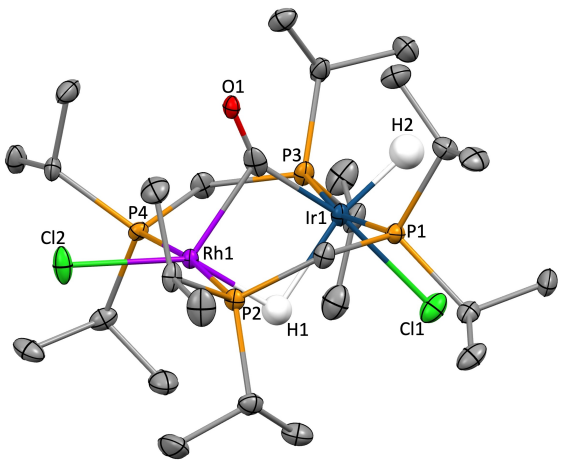

Figure 7. Molecular structure [IrRh(Cl)$_2$(H)(μ-H)(H)(μ-CO)(dppm)$_2$]·(**3**). Thermal ellipsoids are drawn at 50% probability level. Carbon bound hydrogen atoms were omitted for clarity. The positions of the hydrido ligands were fixed at a given position and refined with restraints. Selected bond lengths [Å] and bond angles [°]: Ir1–Rh1 2.8314(5); Ir1–C1 1.926(8); Rh1–C1 2.039(7); C1–Ir1–Cl1 167.9(2); C1–Rh1–Cl2 123.5(2).

Research Article
doi.org/10.1002/ejic.202300099

1,2-difluorobenzene except for the iridium rhodium complex $\mathbf{2c_{IrRh}}$, because of the impurity with the homobimetallic complex $\mathbf{2c_{RhRh}}$ (Scheme 5). When using the bis(diphenylphosphino)methane complex $\mathbf{2a_{IrRh}}$ as precatalyst and sodium *tert*-butoxide as base in thf-d_8 at 80 °C for 2 days, the generation of fluorobenzene and benzene with yields of 15% and 4% was observed (Table 1, entry 1). The bis(di-iso-propylphosphino)methane complexes $\mathbf{2b_{IrRh}}$ and **3** gave a yield of fluorobenzene of only 8% and 3%, respectively (Table 1, entries 2 and 6). The 2-(di-iso-propylphosphino)imidazole complex $\mathbf{2d_{IrRh}}$ performed similarly to $\mathbf{2b_{IrRh}}$ with a yield of 8%. The homobimetallic complex $\mathbf{2a_{RhRh}}$ performed markedly better than heterobimetallic $\mathbf{2a_{IrRh}}$ (64% vs. 19% conversion). Finally, the most active precatalyst was $\mathbf{2c_{RhRh}}$. It resulted in the full conversion of the substrate, a yield of 88% benzene, and an overall TON of 38 (Table 1, entry 5). Complex $\mathbf{2c_{RhRh}}$ exhibits an activity comparable to that reported for the bimetallic In/Rh catalyst by Lu et al. (Scheme 1).[1b] Thus, by using a homodinuclear Rh complex instead of heterodinuclear Ir/Rh complexes, better results in hydrodefluorination were obtained. Notably, the catalysts described here and the compounds by Lu et al. are the only two examples known where dihydrogen was used as reductant for the homogeneous hydrodefluorination of lower-fluorinated aryl fluorides. At lower temperatures (20 °C), almost no conversion, and without any base no reactivities were observed when using $\mathbf{2c_{RhRh}}$. In a control experiment, either without precatalyst $\mathbf{2c_{RhRh}}$ or without dihydrogen, no reactivity was observed (Table 1, entries 7–10). To prove that the binuclearity of the complexes is required, all monometallic complexes **1a**–$\mathbf{d_{Ir}}$ and $\mathbf{1c_{Rh}}$ were also tested. No reactivities were observed for the Ir complexes and only traces of fluorobenzene (~2%) were detected when using $\mathbf{1c_{Rh}}$. Note that mono- and bimetallic Rh hydrido complexes were applied in hydrodefluorination reactions of highly fluorinated aromatic compounds.[23a,26]

To survey the scope of the most efficient catalyst $\mathbf{2c_{RhRh}}$, a variety of fluoroarenes were examined using the standard conditions from the 1,2-difluorobenzene optimization (Scheme 6). Fluorobenzene and *para*-fluoroanisole could be converted into benzene and anisole after 2 days with a yield of 98% and 90%, respectively. For the hydrodefluorination of *para*-fluorotoluene, an extension of the reaction time to 4 days is needed to get a conversion of 96%. With the more electron-poor *para*-fluorotrifluorotoluene, a quantitative hydrodefluorination occurred after 1 day to yield trifluorotoluene, demonstrating that $\mathbf{2c_{RhRh}}$ activates selectively the aryl C–F bond. Finally, 1-fluoro-4-iodobenzene as substrate was tested, showing a preference for cleaving the weaker C–I bond over the C–F bond.

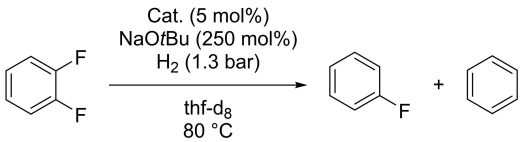

Scheme 5. Hydrodefluorination of 1,2-difluorobenzene with dihydrogen as reductant.

Table 1. Activity of the complexes $\mathbf{2a_{IrRh}}$, $\mathbf{2b_{IrRh}}$, $\mathbf{2d_{IrRh}}$, $\mathbf{2a_{RhRh}}$, $\mathbf{2c_{RhRh}}$ and **3** in catalytic hydrodefluorination under various conditions.[a]

Entry	Precatalyst	Yield C_6H_5F[b] [%]	Yield C_6H_6[b] [%]	Conversion[b] [%]
1	$\mathbf{2a_{IrRh}}$	15	4	19
2	$\mathbf{2b_{IrRh}}$	8	3	10
3	$\mathbf{2d_{IrRh}}$	8	3	10
4	$\mathbf{2a_{RhRh}}$	55	9	64
5	$\mathbf{2c_{RhRh}}$	13	88	100
6	**3**	3	0	3
7[c]	$\mathbf{2c_{RhRh}}$	3	0	3
8[d]	$\mathbf{2c_{RhRh}}$	0	0	0
9[e]	$\mathbf{2c_{RhRh}}$	0	0	0
10	–	0	0	0

[a] Reaction conditions, unless otherwise noted: 1,2-difluorobenzene (0.06 mmol), NaO*t*Bu (0.15 mmol), thf-d_8 (0.6 mL), trifluorotoluene (0.05 mmol) as internal standard, H_2 (1.3 bar), 80 °C, 2 d. [b] The yields were determined by ^{19}F NMR spectroscopy using the integrals of the signals of the internal standard and the substrate or product; duplicate runs were performed. [c] At 20 °C. [d] Without base. [e] Without dihydrogen.

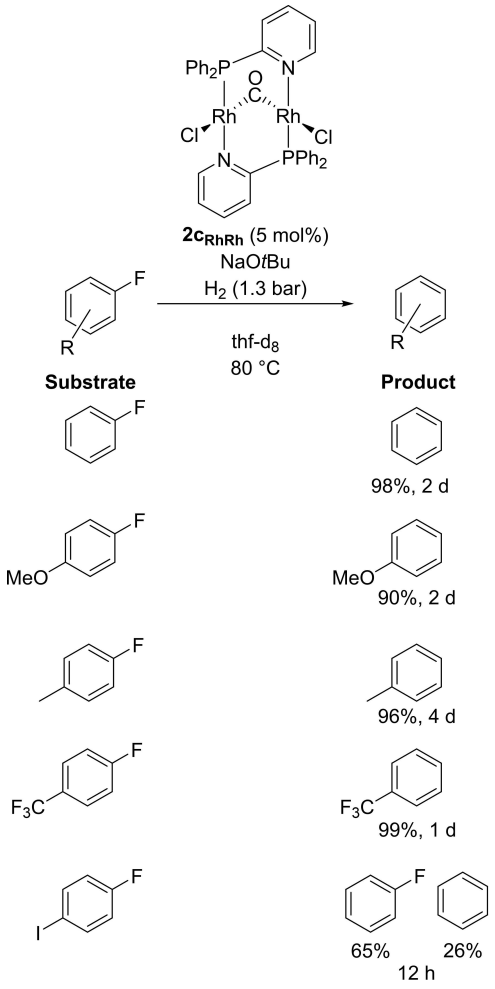

Scheme 6. Hydrodefluorination of fluoroarenes using complex $\mathbf{2c_{RhRh}}$. Reaction conditions: fluorinated benzene derivative (0.06 mmol), NaO*t*Bu (0.09 mmol), thf-d_8 (0.6 mL), trifluorotoluene (0.05 mmol) as internal standard, H_2 (1.3 bar), 80 °C.

Research Article
doi.org/10.1002/ejic.202300099

Examination of solvent-accessible molecular surfaces of the mono- and bimetallic complexes highlights the steric role of the substituents and allows to tentatively contribute to a rationalization of the reactivities of the species with otherwise comparable metal-ligand arrangements. A non-specific access of a reagent with the size of a water molecule to the metal centers and their 1st-shell ligands in the complexes studied here can be qualitatively ranked as follows: $\mathbf{2c}_{RhRh} \approx \mathbf{2c}_{IrRh} \approx \mathbf{2d}_{IrRh} > \mathbf{2a}_{RhRh} \approx \mathbf{2a}_{IrRh} > \mathbf{2b}_{IrRh} \approx \mathbf{3}$ and $\mathbf{1c}_{Rh} \approx \mathbf{1c}_{Ir} > \mathbf{1d}_{Ir} > \mathbf{1a}_{Ir} > \mathbf{1b}_{Ir}$ for the binuclear Ir/Rh and mononuclear Ir- or Rh-only systems. All the surfaces are shown in detail in Figures S42–S44, and for the high vs low access bimetallic complexes ($\mathbf{2c}_{RhRh} \approx \mathbf{2c}_{IrRh} \gg \mathbf{2b}_{IrRh}$) in Figure 8. Complexes $\mathbf{2c}_{RhRh}$, $\mathbf{2c}_{IrRh}$ and $\mathbf{2d}_{IrRh}$ stand out here, showing the largest solvent-accessible metal-bound carbon area. Notably, $\mathbf{2c}_{RhRh}$ also exhibits the best performance in hydrodefluorination (Table 1, entry 5), but no data for $\mathbf{2c}_{IrRh}$ are available (see above). The accessibility in $\mathbf{2c}_{RhRh}$ and $\mathbf{2c}_{IrRh}$ is facilitated by the two Ir/Rh–py planar ring fragments, and similarly in $\mathbf{2d}_{IrRh}$ by the Rh–Im fragments. In contrast, in complexes $\mathbf{2b}_{IrRh}$, **3** and $\mathbf{1b}_{Ir}$ the isopropyl substituents strongly shield the metal centers and their immediate environment. The low catalytic activity of $\mathbf{2d}_{IrRh}$ might possibly be attributed to a higher activity of homobinuclear Rh/Rh complexes when compared to their heterobinuclear Ir/Rh variants, as well as possibly to the tendency of the Ir/Rh–CO ligand in $\mathbf{2d}_{IrRh}$ to form an intermolecular hydrogen bond.

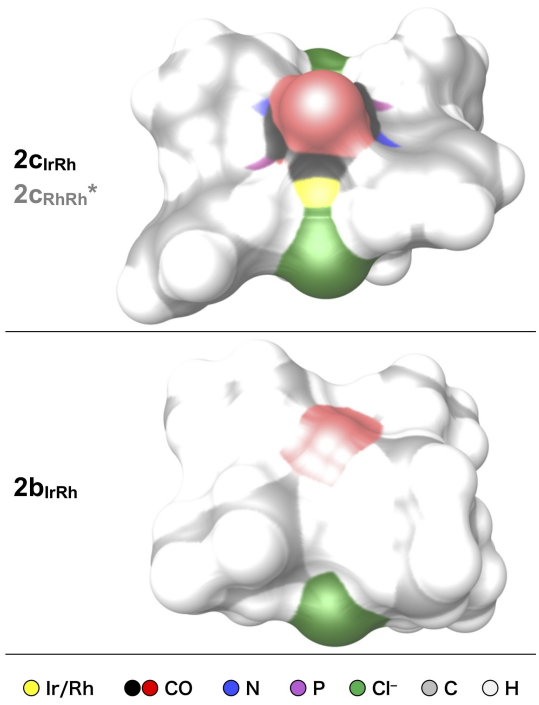

Figure 8. Molecular surfaces of the bimetallic complexes $\mathbf{2c}_{IrRh}$ (top) and $\mathbf{2b}_{IrRh}$ (bottom) based on their optimized DFT structures and created as described in the Supporting Information. (*) The $\mathbf{2c}_{RhRh}$ surface is very similar to its $\mathbf{2c}_{IrRh}$ analogue. The atomic color codes are explained in the bottom row. Surfaces for all the species computationally studied are shown in detail in Figures S42–S44.

Conclusions

In conclusion, synthetic routes to access various bimetallic iridium and rhodium complexes bearing CO bridging ligands have been developed. These bimetallic complexes work efficiently as catalysts in the hydrodefluorination of aryl fluorides, using molecular hydrogen as a reductant and sodium *tert*-butoxide as a base. The results show that the use of two late transition metal centers instead of one is a viable strategy for the activation of strong C–F bonds. A superior exposure of the Ir/Rh centers might tentatively be associated with the catalytic efficiency.

Experimental Section

Details of experimental procedures and computational methods, characterization of the complexes, NMR and IR data, supplementary DFT results and figures, Cartesian coordinates of the optimized structures can be found in the Supporting Information.

Deposition Numbers 2180874 (for $\mathbf{1a}_{Ir}\cdot H_2O$), 2180873 (for $\mathbf{1b}_{Ir}\cdot$dcm), 2180878 (for $\mathbf{1c}_{Ir}\cdot$dcm), 2180875 (for $\mathbf{2a}_{IrRh}\cdot$dcm), 2180877 (for $\mathbf{2c}_{IrRh}\cdot 4\,C_6D_6$), 2180872 (for **3**) contain the supplementary crystallographic data for this paper. These data are provided free of charge by the joint Cambridge Crystallographic Data Centre and Fachinformationszentrum Karlsruhe Access Structures service.

Acknowledgements

This work was funded by the Deutsche Forschungsgemeinschaft (DFG, German Research Foundation) under Germany's Excellence Strategy – EXC 2008 – 390540038 – UniSysCat. Open Access funding enabled and organized by Projekt DEAL.

Conflict of Interest

The authors declare no conflict of interest.

Data Availability Statement

The data that support the findings of this study are available in the supplementary material of this article.

Keywords: aryl fluorides · bimetallic · hydrodefluorination · iridium · rhodium

[1] a) S. Sabater, J. A. Mata, E. Peris, *Nat. Commun.* **2013**, *4*, 2553; b) J. T. Moore, C. C. Lu, *J. Am. Chem. Soc.* **2020**, *142*, 11641–11646; c) A. Zanardi, J. A. Mata, E. Peris, *J. Am. Chem. Soc.* **2009**, *131*, 14531–14537; d) A. Zanardi, J. A. Mata, E. Peris, *Chem. Eur. J.* **2010**, *16*, 13109–13115; e) J. A. Mata, F. E. Hahn, E. Peris, *Chem. Sci.* **2014**, *5*, 1723–1732; f) Y. Zhang, S. P. Roberts, R. G. Bergman, D. H. Ess, *ACS Catal.* **2015**, *5*, 1840–1849; g) J. Coombs, D. Perry, D.-H. Kwon, C. M. Thomas, D. H. Ess, *Organometallics* **2018**, *37*, 4195–4203; h) K. M. Gramigna, D. A. Dickie, B. M. Foxman, C. M. Thomas, *ACS Catal.* **2019**, *9*, 3153–3164; i) J. Campos, *Nat. Chem. Rev.* **2020**, *4*, 696–702; j) A. C. Deacy, A. F. R. Kilpatrick, A. Regoutz,

C. K. Williams, *Nat. Chem.* **2020**, *12*, 372–380; k) M. J. Dorantes, J. T. Moore, E. Bill, B. Mienert, C. C. Lu, *Chem. Commun.* **2020**, *56*, 11030–11033; l) M. V. Vollmer, J. Ye, J. C. Linehan, B. J. Graziano, A. Preston, E. S. Wiedner, C. C. Lu, *ACS Catal.* **2020**, *10*, 2459–2470; m) V. Cherepakhin, A. Hellman, Z. Lan, S. Mallikarjun Sharada, T. J. Williams, *Dalton Trans.* **2020**, *49*, 10509–10515; n) J. T. Moore, M. J. Dorantes, Z. Pengmei, T. M. Schwartz, J. Schaffner, S. L. Apps, C. A. Gaggioli, U. Das, L. Gagliardi, D. A. Blank, C. C. Lu, *Angew. Chem. Int. Ed. Engl.* **2022**, *61*, e202205575; *Angew. Chem.* **2022**, *134*, e202205575.

[2] a) B. A. Vaartstra, J. Xiao, J. A. Jenkins, R. Verhagen, M. Cowie, *Organometallics* **1991**, *10*, 2708–2717; b) F. Antwi-Nsiah, M. Cowie, *Organometallics* **1992**, *11*, 3157–3160; c) B. A. Vaartstra, M. Cowie, *Organometallics* **1989**, *8*, 2388–2394; d) R. W. Hilts, O. Oke, M. J. Ferguson, R. McDonald, M. Cowie, *Organometallics* **2005**, *24*, 4393–4405; e) R. McDonald, M. Cowie, *Inorg. Chem.* **1990**, *29*, 1564–1571; f) R. W. Hilts, R. A. Franchuk, M. Cowie, *Organometallics* **1991**, *10*, 1297–1304; g) T. J. MacDougall, M. J. Ferguson, R. McDonald, M. Cowie, *Organometallics* **2012**, *31*, 4516–4528; h) F. H. Antwi-Nsiah, O. Oke, M. Cowie, *Organometallics* **1996**, *15*, 506–520; i) M. H. Mobarok, R. McDonald, M. J. Ferguson, M. Cowie, *Inorg. Chem.* **2012**, *51*, 4020–4034; j) A. T. Hutton, P. G. Pringle, B. L. Shaw, *Organometallics* **1983**, *2*, 1889–1891; k) F. H. Antwi-Nsiah, O. Oke, M. Cowie, *Organometallics* **1996**, *15*, 1042–1054; l) O. Oke, R. McDonald, M. Cowie, *Organometallics* **1999**, *18*, 1629–1640; m) B. D. Rowsell, S. J. Trepanier, R. Lam, R. McDonald, M. Cowie, *Organometallics* **2002**, *21*, 3228–3237; n) M. M. Dell'Anna, S. J. Trepanier, R. McDonald, M. Cowie, *Organometallics* **2001**, *20*, 88–99; o) B. A. Vaartstra, M. Cowie, *Inorg. Chem.* **1989**, *28*, 3138–3147; p) M. H. Mobarok, M. J. Ferguson, M. Cowie, *Organometallics* **2012**, *31*, 4722–4728; q) J. R. Torkelson, O. Oke, J. Muritu, R. McDonald, M. Cowie, *Organometallics* **2000**, *19*, 854–864; r) D. S. A. George, R. McDonald, M. Cowie, *Organometallics* **1998**, *17*, 2553–2566; s) T. Braun, A. Steffen, V. Schorlemer, B. Neumann, H.-G. Stammler, *Dalton Trans.* **2005**, 3331–3336; t) D. S. A. George, R. W. Hilts, R. McDonald, M. Cowie, *Inorg. Chim. Acta* **2000**, *300–302*, 353–368; u) R. McDonald, M. Cowie, *Inorg. Chem.* **1993**, *32*, 1671–1680; v) D. S. A. George, R. W. Hilts, R. McDonald, M. Cowie, *Organometallics* **1999**, *18*, 5330–5343.

[3] a) G. Franciò, R. Scopelliti, C. G. Arena, G. Bruno, D. Drommi, F. Faraone, *Organometallics* **1998**, *17*, 338–347; b) S.-M. Kuang, F. Xue, Z.-Z. Zhang, W.-M. Xue, C.-M. Che, T. C. W. Mak, *J. Chem. Soc. Dalton Trans.* **1997**, 3409–3410.

[4] M. Cowie, S. K. Dwight, *Inorg. Chem.* **1980**, *19*, 2500–2507.

[5] a) D. J. Anderson, R. McDonald, M. Cowie, *Angew. Chem. Int. Ed.* **2007**, *46*, 3741–3744; *Angew. Chem.* **2007**, *119*, 3815–3818; b) M. E. Slaney, M. J. Ferguson, R. McDonald, M. Cowie, *Organometallics* **2012**, *31*, 1384–1396.

[6] a) J. L. Kiplinger, T. G. Richmond, C. E. Osterberg, *Chem. Rev.* **1994**, *94*, 373–431; b) H. Amii, K. Uneyama, *Chem. Rev.* **2009**, *109*, 2119–2183; c) A. Nova, R. Mas-Ballesté, A. Lledós, *Organometallics* **2011**, *31*, 1245–1256; d) M. F. Kuehnel, D. Lentz, T. Braun, *Angew. Chem. Int. Ed.* **2013**, *52*, 3328–3348; *Angew. Chem.* **2013**, *125*, 3412–3422; e) T. Stahl, H. F. T. Klare, M. Oestreich, *ACS Catal.* **2013**, *3*, 1578–1587; f) T. Ahrens, J. Kohlmann, M. Ahrens, T. Braun, *Chem. Rev.* **2015**, *115*, 931–972; g) T. A. Unzner, T. Magauer, *Tetrahedron Lett.* **2015**, *56*, 877–883; h) O. Eisenstein, J. Milani, R. N. Perutz, *Chem. Rev.* **2017**, *117*, 8710–8753; i) J. D. Hamel, J. F. Paquin, *Chem. Commun.* **2018**, *54*, 10224–10239; j) N. O. Andrella, N. Xu, B. M. Gabidullin, C. Ehm, R. T. Baker, *J. Am. Chem. Soc.* **2019**, *141*, 11506–11521; k) T. Fujita, K. Fuchibe, J. Ichikawa, *Angew. Chem. Int. Ed.* **2019**, *58*, 390–402; *Angew. Chem.* **2019**, *131*, 396–408; l) M. Ohashi, S. Ogoshi, in *Organometallic Fluorine Chemistry* (Eds.: T. Braun, R. P. Hughes), Springer International Publishing, Cham, **2015**, pp. 197–215; m) M. Talavera, T. Braun, *Synlett* **2020**, *31*, 1760–1774; n) T. Braun, F. Wehmeier, *Eur. J. Inorg. Chem.* **2011**, 613–625; o) G. Meier, T. Braun, *Angew. Chem. Int. Ed.* **2009**, *48*, 1575–1577; *Angew. Chem.* **2009**, *121*, 1546–1548; p) M. Talavera, C. N. von Hahmann, R. Müller, M. Ahrens, M. Kaupp, T. Braun, *Angew. Chem. Int. Ed.* **2019**, *58*, 10688–1069; *Angew. Chem.* **2019**, *131*, 10798–10802; q) L. Keyes, J. A. Love, in *C–H and C–X Bond Functionalization: Transition Metal Mediation* (Eds.: X. Ribas), The Royal Society of Chemistry, **2013**.

[7] J. S. Miller, K. G. Caulton, *J. Am. Chem. Soc.* **1975**, *97*, 1067–1073.

[8] A. K. Jain, M. R. Gau, P. J. Carroll, K. I. Goldberg, *Chem. Sci.* **2022**, *13*, 7837–7845.

[9] a) J. O. Yu, E. Lam, J. L. Sereda, N. C. Rampersad, A. J. Lough, C. S. Browning, D. H. Farrar, *Organometallics* **2005**, *24*, 37–47; b) J. O. Yu, C. Scott Browning, D. H. Farrar, *Chem. Commun.* **2008**, 1020–1022; c) Y.-Y. Kuo, M. F. Haddow, A. Pérez-Redondo, G. R. Owen, *Dalton Trans.* **2010**, *39*, 6239–6248.

[10] a) S. A. Cotton, in *Chemistry of Precious Metals*, Springer Netherlands, Dordrecht, **1997**, pp. 78–172; b) L. D. Field, E. T. Lawrenz, A. J. Ward, *Polyhedron* **1999**, *18*, 3031–3034; c) A. Tahara, Y. Miyamoto, R. Aoto, K. Shigeta, Y. Une, Y. Sunada, Y. Motoyama, H. Nagashima, *Organometallics* **2015**, *34*, 4895–4907.

[11] J. P. Farr, M. M. Olmstead, C. H. Hunt, A. L. Balch, *Inorg. Chem.* **1981**, *20*, 1182–1187.

[12] a) B. R. James, D. Mahajan, *Can. J. Chem.* **1980**, *58*, 996–1004; b) L. H. Pignolet, D. H. Doughty, S. C. Nowicki, A. L. Casalnuovo, *Inorg. Chem.* **1980**, *19*, 2172–2177.

[13] J. Wolf, M. Manger, U. Schmidt, G. Fries, D. Barth, B. Weberndörfer, D. A. Vicic, W. D. Jones, H. Werner, *J. Chem. Soc. Dalton Trans.* **1999**, 1867–1876.

[14] J. A. J. Jarvis, R. H. B. Mais, P. G. Owston, K. A. Taylor, *Chem. Commun.* **1966**, 906b–908.

[15] A. W. Addison, T. N. Rao, J. Reedijk, J. Van Rijn, G. C. Verschoor, *J. Chem. Soc. Dalton Trans.* **1984**, 1349–1356.

[16] M. Rowen Churchill, J. C. Fettinger, L. A. Buttrey, M. D. Barkan, J. S. Thompson, *J. Organomet. Chem.* **1988**, *340*, 257–266.

[17] A. Conkie, E. A. V. Ebsworth, R. A. Mayo, S. Moreton, *J. Chem. Soc. Dalton Trans.* **1992**, 2951–2954.

[18] N. Pfister, T. Braun, P. Wittwer, M. Ahrens, *Z. Anorg. Allg. Chem.* **2018**, *644*, 1064–1070.

[19] K. Wajda-Hermanowicz, F. P. Pruchnik, *Transition Met. Chem.* **1988**, *13*, 101–103.

[20] a) H. A. Mayer, W. C. Kaska, *Chem. Ber.* **1995**, *128*, 95–98; b) J. K. MacDougall, M. C. Simpson, M. J. Green, D. J. Cole-Hamilton, *J. Chem. Soc. Dalton Trans.* **1996**, 1161–1172; c) J. Rankin, A. C. Benyei, D. J. Cole-Hamilton, A. D. Poole, *Chem. Commun.* **1997**, 1835–1836.

[21] a) J. T. Mague, *Organometallics* **1986**, *5*, 918–926; b) J. T. Mague, A. R. Sanger, *Inorg. Chem.* **1979**, *18*, 2060–2066.

[22] S. J. Young, B. Kellenberger, J. H. Reibenspies, S. E. Himmel, M. Manning, O. P. Anderson, J. K. Stille, *J. Am. Chem. Soc.* **1988**, *110*, 5744–5753.

[23] a) T. Braun, D. Noveski, M. Ahijado, F. Wehmeier, *Dalton Trans.* **2007**, 3820–3825; b) M. K. Cybulski, I. M. Riddlestone, M. F. Mahon, T. J. Woodman, M. K. Whittlesey, *Dalton Trans.* **2015**, *44*, 19597–19605; c) M. K. Cybulski, C. J. E. Davies, J. P. Lowe, M. F. Mahon, M. K. Whittlesey, *Inorg. Chem.* **2018**, *57*, 13749–13760.

[24] a) H. Schumann, M. Heisler, J. Pickardt, *Chem. Ber.* **1977**, *110*, 1020–1026; b) P. Cheliatsidou, D. F. White, A. M. Slawin, D. J. Cole-Hamilton, *Dalton Trans.* **2008**, 2389–2394; c) R. Jaeger, M. Talavera, T. Braun, *J. Fluorine Chem.* **2021**, *247*, 109803.

[25] R. McDonald, B. R. Sutherland, M. Cowie, *Inorg. Chem.* **1987**, *26*, 3333–3339.

[26] a) L. Zámostná, M. Ahrens, T. Braun, *J. Fluorine Chem.* **2013**, *155*, 132–142; b) S. I. Kalläne, M. Teltewskoi, T. Braun, B. Braun, *Organometallics* **2015**, *34*, 1156–1169; c) L. Zamostna, S. Sander, T. Braun, R. Laubenstein, B. Braun, R. Herrmann, P. Klaring, *Dalton Trans.* **2015**, *44*, 9450–9469; d) L. Schwartsburd, M. F. Mahon, R. C. Poulten, M. R. Warren, M. K. Whittlesey, *Organometallics* **2014**, *33*, 6165–6170; e) J. Chen, D. Huang, Y. Ding, *ChemistrySelect* **2017**, *2*, 1219–1224.

Manuscript received: February 23, 2023
Revised manuscript received: March 2, 2023
Accepted manuscript online: March 2, 2023